Int. J. Pharm. Investigation, 2026; 16(1):210-224.
https://www.jpionline.org

Original Article

Exploring the Bioactivity of Zinc Oxide Nanoparticles Synthesized Using *Kigelia africana* Fruit Extract

Dharshini Jaisankar Hindumathi[1], Jubilee Ramasamy[1,*], Deepika Jothibasu[1], Niranjani Ravikumar[1], Binoy Varghese Cheriyan[2], Kaniga Pandi[2]

[1]Department of Pharmacology, Saveetha College of Pharmacy, Saveetha Institute of Medical and Technical Sciences (SIMATS), Saveetha University, Chennai, Tamil Nadu, INDIA.
[2]Department of Pharmaceutical Chemistry, Saveetha College of Pharmacy, Saveetha Institute of Medical and Technical Sciences (SIMATS), Saveetha University, Chennai, Tamil Nadu, INDIA.

ABSTRACT

Background: Nanoparticles are nanoscale materials that are well known for their distinct physical and chemical characteristics. Owing to their tiny size and special characteristics, nanoparticles such as zinc oxide nanoparticles are widely prized for their use in medicine, especially for antioxidant and antibacterial applications. **Materials and Methods:** This study focused on ZnONP synthesized from *Kigelia africana* fruit extract (Sausage tree), which is rich in bioactive compounds such as alkaloids, flavonoids, and saponins. The characterization of the biosynthesized ZnONP included UV-visible spectroscopy, FTIR, XRD, SEM and EDXS. Free radical scavenge is evaluated across various antioxidant assays, such as DPPH, H_2O_2, ABTS, NO_2, and FRAP. **Results and Discussion:** UV-visible spectroscopy confirmed the synthesis of ZnONP with an absorption peak at 340 nm; FTIR identified functional groups (O-H, H-O-H, C-O, and Zn-O); XRD revealed a crystalline structure with prominent peaks and particle sizes ranging from 113 to 884; SEM revealed an aggregated morphology; and EDXS confirmed the presence of zinc, oxygen and carbon. ZnONP showed potent free radical scavenging across various antioxidant assays, such as DPPH (inhibition: 89.47%; IC_{50}: 19.01 µg/mL), H_2O_2 (inhibition: 85.6%; IC_{50}: 1.7 µg/mL), ABTS (inhibition: 91.23%; IC_{50}: 8.85 µg/mL), NO_2 (inhibition: 87.21%; IC_{50}: 28.06 µg/mL) and FRAP (inhibition: 89.54%; IC_{50}: 26.54 µg/mL) assays. The zone of inhibition around the ZnONP-treated wells demonstrated antibacterial efficacy. These tests collectively demonstrate that the ZnONP have strong antioxidant effects, antibacterial effects, and structural integrity. Owing to their antioxidant qualities, which improved bacterial cell disintegration and sustained antibacterial effects, *Kigelia africana* ZnONP demonstrated significant antibacterial effects, highlighting their potential for long-term biomedical applications.

Keywords: Antibacterial, Antioxidant, *Kigelia africana*, Nanoparticles, Zinc oxide.

Correspondence:
Dr. Jubilee Ramasamy
Associate Professor, Department of Pharmacology, Saveetha College of Pharmacy, Saveetha Institute of Medical and Technical Sciences (SIMATS), Saveetha University, Chennai-601205, Tamil Nadu, INDIA.
Email: jubliee.cology@gmail.com

Received: 28-05-2025;
Revised: 03-07-2025;
Accepted: 16-09-2025.

INTRODUCTION

NP (Nano Particles) can be produced via physical, chemical, or biological methods. Biological approaches have more potential because they are economic and environmentally friendly. In biological methods, microorganisms or medicinal plants are used to produce nanoparticles (Dua *et al.*, 2023). Medical plants are advantageous because their therapeutic properties are added to the NPs during synthesis. Plant phytocompounds provide antioxidant properties, and plants with antibacterial activity provide additional antioxidant properties to NPs (Jeyabharathi *et al.*, 2022). Zinc oxide has been utilized as an antibacterial agent, and zinc-based compounds are less expensive than gold-based compounds. Furthermore, (ZnONP) (zinc oxide nanoparticles) are highly toxic to prokaryotic cells, such as bacteria, fungi, and viruses, but are nontoxic to eukaryotic cells, i.e., human cells. ZnONP possess unique physical, chemical, magnetic, electrical, and mechanical characteristics (Sorbiun *et al.*, 2018). Owing to these unique properties, researchers are interested in exploring its applications in nanomedicines, such as antibacterial, antiplasmodial, targeted drug delivery, antifungal, anticancer, antiplatelet, and wound healing activities (Demissie *et al.*, 2020). Improvements in the synthesis of zinc oxide nanoparticles have significantly impacted several scientific fields. Owing to their low yield and use of toxic substances, zinc oxide nanoparticles are not synthesized via physical or chemical methods (Kokate *et al.*, 2016). Numerous studies have reported that plant extracts used to synthesize ZnONP include *Cayratia pedate* (Jayachandran *et al.*, 2021), *Aloe vera* (Manikanika and Chopra, 2023), *curcumin* (Perera *et al.*, 2020), *Limonia acidissima* (Patil and Taranath, 2016), *Justicia adhatoda* (Pachaiappan *et al.*, 2021), *Brassica oleracea*

DOI: 10.5530/ijpi.20260318

(Wali *et al*., 2024), *Geranium wallichianum* (Abbasi *et al*., 2020), *Melia azedarach* (Dhandapani *et al*., 2020), *Caaia alata* (Happy *et al*., 2019), *Raphanus sativus* (Al Awadh *et al*., 2022), *Anoectochilus elatus* (Vijayakumar *et al*., 2022), *Cinnamomum tamala* (Narath *et al*., 2021), *and Phoenix dactylifera* (Jency Evanjelin *et al*., 2023). *Kigelia africana* fruit, commonly known as the sausage tree, belongs to the Bignoniaceae family and is rich in bioactive components such as alkaloids, steroids, quinones, iridoids and phenolic compounds (Houghton and Jâger, 2002). *Kigelia africana* fruit extract has antioxidant, antibacterial, antifungal, and anti-inflammatory properties; has antitumour activity; and is frequently used to treat diabetes, infertility, liver-borne disease, etc., (Osman *et al*., 2017). For the abovementioned reasons, the present study intended to use extracts from *Kigelia africana* fruit to synthesize ZnONPs and evaluate their antioxidant activity and antibacterial effects against pathogenic bacteria such as *E. faecalis, E. coli, S. aureus, and Klebsiella* sp.

MATERIALS AND METHODS

Plant collection

Fruits of *Kigelia africana* were collected from Central Africa. The collected fruits were authenticated by Prof. Dr. P. Jayaraman, Ph.D., The Director, Plant Anatomy Research Centre (PARC), Pharmacognosy Institute, West Thambaram, Chennai (Ref no: PARC/2020/4253).

Extraction

The dried *Kigelia africana* fruits were crushed into a coarse powder via an electric grinder. The powdered materials were separately soaked in 25 L of hydro ethanol solution (2:8) for 7 days. This process, known as maceration, allows the solvent to dissolve the desired compounds from the plant material. The mixture was stirred regularly to ensure uniform extraction. After 7 days, the extracts were filtered to remove any solid residues via Whatman no. 4 filter paper. The clarified extracts were then concentrated via an evaporator (rotary evaporator). The concentrated extracts were dried in a laboratory oven at 45°C to remove any remaining solvent, leaving behind a dry extract (Arena *et al*., 2020).

ZnO nanoparticle synthesis

A solution of 30 mmol/L ZnS was made by mixing the appropriate quantity of ZnS in 70 mL of distilled water. 30 mL of plant extract was added to 70 mL of ZnS solution, and the mixture was stirred continuously. The mixture was then incubated at 37°C for 48 hr, which is a common temperature for biological reactions and a time period that allows the reaction to proceed to completion. After incubation, the mixture was allowed to rest at room temperature for an unspecified period, which allowed the ZnO nanoparticles to precipitate out of the solution. The precipitated nanoparticles were separated from the solution by centrifuging the mixture at 10,000 rpm for 5 min. The precipitate was washed twice with distilled water to filter impurities and then dried at 80°C. The dried powder of the ZnO nanoparticles was scraped (I *et al*., 2023).

Characterization of ZnONP

Several analytical techniques were used to confirm the shape, size, and morphology of the synthesized ZnONP. Some of these techniques include UV-visible spectroscopy, Fourier Transform Infrared (FTIR) spectroscopy, X-ray Diffraction (XRD), and Scanning Electron Microscopy (SEM), and energy dispersive X-ray Spectroscopy (EDXS).

UV-vis Spectroscopy

UV-vis spectroscopy is based on the transition of electrons from the ground state to the excited state in response to electromagnetic waves. The spectra within the electromagnetic wave range of 1.5 eV to 6.2 eV correspond to wavelengths ranging from 800 to 200 nm. At room temperature, the optical characteristics of the ZnONP were determined by a UV-vis spectrophotometer. The spectral analysis was carried out at a resolution of 1 nm in the 800-200 nm range (Urnukhsaikhan *et al*., 2021).

Fourier Transform Infrared Spectroscopy

FTIR (or Fourier transform infrared) spectroscopy confirmed the functional groups associated with the synthesis of the ZnONP. For analysis, ZnONP powder was mixed with KBr and compressed at 11,000 psi to create a disc. The detector is connected via clean dry nitrogen gas to reduce moisture and increase the signal level. The disc was introduced into the spectrophotometer, and the spectra were measured within the range of 4000 cm^{-1}-500 cm^{-1} and examined via online spectroscopic analysis (Dlamini *et al*., 2023).

X-ray Diffraction

An X-ray diffractometer was used to carry out the XRD analysis. The X-ray source for the diffraction had a wavelength of 1.20 angstroms (Å). The 2θ for XRD scanning was within the range of 10-80°. This range is set by several diffraction peaks that may be present and active for the purpose of identifying the crystalline phases in the samples. The applied voltage and current are optimized for the operating conditions: 40 kV and 40 mA, respectively. Theoretically, while the voltage determines the energy of the X-ray beam, the current determines the intensity. All are optimized by good diffraction without any incident on the sample. A divergence slit refers to an aperture used to set the beam width. A 0.3 mm slit is used to set the beam's divergence in the plane perpendicular to the sample surface. The notation 2θ/θ expresses that the incident X-ray beam-to-detector angle is changed at the same time, i.e., such that the angle, 2θ, remains constant (Nouren *et al*., 2024).

Scanning electron microscopy

One of the most common techniques applied to image the surface morphology, shape, and size of a large variety of materials, including nanoparticles, is scanning electron microscopy. A much diluted suspension of the nanoparticles is prepared so that the particles are spread out in the suspension and do not agglomerate on the grid. The suspension was sonicated for 5 min to provide good dispersion. A drop of the sonicated suspension was placed on a gold grid, an attractive substrate for SEM imaging because it is conductive. The sample was then left to dry for 15 min. In this case, the solvent evaporates, leaving behind the nanoparticles on the grid. After that, the dried sample was loaded onto the pattern holder, a device designed for holding samples in place against the imaging action. The holder was designed such that it can fit in the SEM chamber and offer a solid stage for the sample to be imaged. After the sample was loaded into the SEM, a fine intense beam was used for scanning. When these impinging electrons interact with the very atoms that make up the sample, they cause several signals, all of which can be detected and used in building images of the surface of a sample. The SEM images provide high resolution and, therefore, a high level of detail related to the shape, size, and morphology of the nanoparticles (Purbowati *et al.*, 2023).

Energy dispersive X-ray spectroscopy

EDXS analysis was used to confirm the elemental compositions produced by the biosynthesized ZnONP. EDXS analysis was carried out with EDX-AMETEX (Ashwini *et al.*, 2021).

Anti-oxidant activity

The antioxidant effects of the ZnONP were evaluated via various scavenging assays: DPPH (2,2-diphenyl-1-picrylhydrazyl), H_2O_2 (hydrogen peroxide), ABTS (azinobis-3-ethylbenzothiazoline-6-sulfonic acid), FRAP (ferric reducing antioxidant power), and NO_2 (nitric oxide).

DPPH Assay

A methanol solution of 0.1 mM DPPH was prepared via a standard protocol. An operational solution was developed for each test by diluting the initial solution with methanol to achieve a final concentration of 20 µM. In a six-well plate, various concentrations (10 µg/mL, 20 µg/mL, 30 µg/mL, 40 µg/mL, and 50 µg/mL) of ZnONP were added to 200 µL of DPPH working solution. The plate was positioned in a poorly illuminated location and kept at normal temperature for 30 min. The absorbance at 517 nm was measured via a microplate reader. Methanol was used as blank solution (Deng *et al.*, 2011).

The DPPH scavenging activity percentage was determined as follows:

$$[(\text{control A} - \text{sample A})/\text{control A}] \times 100$$

where

Control A: Absorbance value of DPPH

Sample A: Absorbance value of DPPH with ZnONP

H_2O_2 Assay

1 mL of 28 mM 2-deoxy-2-ribose was added to formulate a reaction mixture. Different concentrations of ZnONPs (10-50 µg/mL) were added. Furthermore, 200 µL of 200 µM $FeCl_3$, 200 µL of EDTA and 100 µL of ascorbic acid were added. The sample was then incubated for approximately 1 hr at 37°C. After incubation, the optical intensity was measured at 532 nm and compared to that of the reference solution. Vitamin-E was used as a positive control (Kayani *et al.*, 2016).

The H_2O_2 scavenging activity percentage was determined as follows:

$$[(\text{blank A} - \text{sample A})/\text{blank A}] \times 100$$

where

Blank A: Absorbance value of the blank

Sample A: Absorbance value of the test

ABTS Assay

Potassium persulfate (2.45 mM) and 7.0 mM ABTS (50% ethanol) were used to generate positive ABTS radical ions (ABTS+). The reagents were stored in a refrigerated setting for 24 hr. Prior to use, the reagent was diluted with 50% ethanol until it reached an absorbance at 734 nm of 1.0 (±0.02). ABTS+ (250 µL) and various chemical concentrations were added to the 96-well microplates. After 10 min of reaction, the absorbance at 734 nm was measured (Re *et al.*, 1999).

The ABTS scavenging activity percentage was determined as follows:

$$[(\text{Abs } 0 - \text{Abs } 1)/\text{Abs } 0] \times 100$$

where

Abs 0: Absorbance of the blank

Abs 1: Absorbance of the Test

NO_2 Assay

The NO_2 assay is estimated via GRIESS ILOSVAY REACTION. In this work, this component is modified by substituting 1-napthylamine (5%) with naphthyl ethylene diamine dihydrochloride (0.1% w/v). Sodium nitroprusside, phosphate-buffered saline and ZnONP or stock solution were combined and incubated for 150 min. Afterward, 0.5 mL of the resulting mixture was combined with 1 mL of sulfanilic acid, and the mixture was allowed to rest for 5 min. 1 mL of naphthyl ethylene diamine dihydrochloride was added, and the mixture was mixed and allowed to rest for 30 min. Under diffuse light;

a pink-colored dye is produced. The absorbance was measured at 540 nm using a blank solution as a reference and rutin as a standard (Singh and Tripathi, 2018).

FRAP Assay

Make 300 mM acetate buffer (pH 3.6) by mixing sodium acetate trihydrate (3.1 g) with glacial acetic acid (16 mL). The FRAP reagent was prepared by combining 10 mM TPTZ with 20 mM ferric chloride in acetate buffer. The standard used here was ferrous sulfate heptahydrate ($FeSO_4 \cdot 7H_2O$) with a concentration of 0.1 to 1.5 mM in methanol. Then, 3.6 mL of FRAP solution was mixed with 0.4 mL of purified water and incubated for 5 min at 37°C. Furthermore, this solution was combined with 80 mL of ZnONP and incubated for 10 min at 37°C. The optical intensity of the mixture was measured at 593 nm. For the standard curve, 5 distinct concentrations of $FeSO_4.7H_2O$ (0.1 mM, 0.4 mM, 0.8 mM, 1 mM, 1.12 mM and 1.5 mM) were used (Thaipong *et al.*, 2006).

Antibacterial activity

ZnONP were evaluated for their antibacterial efficacy against various bacteria, such as *E. coli, E. faecalis, S. aureus, and Klebsiella sp*., via the agar well diffusion technique. The procedure involves sterilizing and solidifying MHA (Mueller-Hinton agar) media, which are routinely used for antibiotic susceptibility testing, by pouring them onto sterile petri plates. Every Petri dish was swabbed with a newly grown culture of a particular strain of bacteria that had been incubated overnight. The synthesized ZnONP were suspended in DMSO (dimethyl sulfoxide) at a concentration of 100 mg/mL. The wells were created in agar, and 25 µL, 50 µL or 100 µL of the ZnONP suspension was added to each well. The plates were incubated at 37°C and incubated undisturbed for 18-24 hr. Chloramphenicol was used as a control in this work. After incubation, the zone of inhibition (the clear area around the well where bacterial growth is inhibited) was measured. This zone represents the effectiveness of the antibacterial agent (Chukwudozie and Ezeonu, 2022)(Anandhi *et al*., 2022).

RESULTS

Characterization of ZnONP

UV-vis Spectroscopy

Figure 1 shows the UV-vis spectroscopy plot of the ZnONP, where the x-axis and y-axis represent the wavelength (nm) and absorbance, respectively.

The graph comprises the measurement data collected at distinct time intervals of 3 hr, 12 hr and 24 hr. The bandgap absorption of the ZnONP is characterized by an absorbance of 340 nm, which is substantial for all 3 time intervals (3 hr, 12 hr and 24 hr). Zinc oxide commonly absorbs UV light between 330 and 370 nm because of its broad bandgap of approximately 3.37 eV, where the peak is visible. At 3 hr, the spectrum reached the maximum absorbance at 340 nm, suggesting that the early phase of nanoparticle development was characterized by a reduced particle size or elevated concentration. After 12 hr, a modest decrease was observed, indicating that the increase in particle size or changes in the nanoparticle structure may impact the optical characteristics. After 24 hr, a further marginal decline in absorbance occurred, suggesting potential further expansion or changes in the particle structure. Nevertheless, the spectrum shows a high degree of consistency, indicating the durability of the optical characteristics of the nanoparticles.

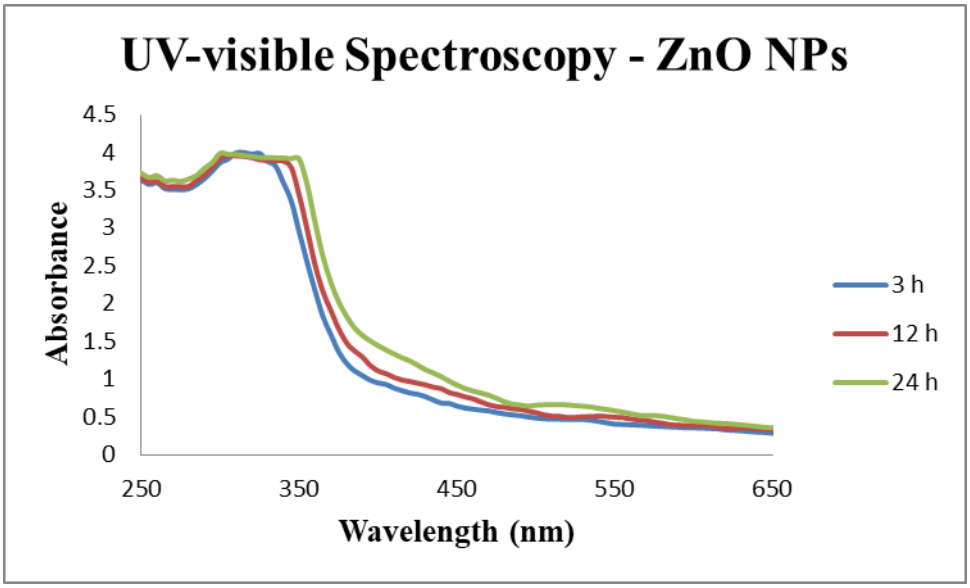

Figure 1: UV-vis spectroscopy of the ZnONPs.

Fourier Transform Infrared Spectroscopy

Figure 2 shows the transmittance spectrum of the ZnONP. FTIR spectra were used to identify the functional groups present in the ZnONP within the range of 4000--500 cm^{-1}. FTIR spectroscopy confirmed the existence of ZnONP at 3194.739 cm^{-1} (O-H stretching vibration, hydroxyl groups or adsorbed water), 1628.567 cm^{-1} (by bending mode of water molecules adsorbed (H-O-H)), 1425.680 cm^{-1} (due to C-H bending or stretching-type vibrations, presence of organic residues, 1066.590 cm^{-1} (C-O stretching vibration, presence of carbonate groups), 525.646 cm^{-1}, 421.489 cm^{-1}, and 400.482 cm^{-1} (characteristic of Zn-O stretching modes, the presence of ZnO), as mentioned in Table 1.

X-ray Diffraction

Figure 3 shows the XRD pattern of ZnONP. The 2θ values of the diffraction peaks range from 15.13°, 16.34°, 17.62°, 18.15°, 18.46°, 20.42°, 21.48°, 22.24°, 22.92°, 23.98°, 24.81°, 25.87°, 26.62°, 28.21°, 29.42°, 30.93°, 31.54°, 32.29°, 33.50°, 34.79°, 36.15°, 37.59°, 39.63°, 40.92°, 43.94°, 45.60°, 49.01°, 50.52°, 52.03°, and 53.24°. The strongest peak is at approximately 20.42°, whereas few other significant peaks are at approximately 22.24° and 30.93°. The Bragg reflections of the prominent peaks are the 31.54° (100), 34.80° (002), 36.16° (101), 43.95° (102), 50.52° (110), and 53.25° (103) planes of the ZnONP structure (standard JCPDS 36--1451), and these peaks confirm the presence of ZnONP. The sharp diffraction pattern confirms the presence of 45.6% and 54.4% crystalline ZnONP. The crystalline size of ZnONP varies across different peaks, and the average size was determined via Scherrer's equation and was observed to be between 20 nm and 40 nm.

Scanning electron microscopy

The surface morphology of ZnONPs was verified via SEM at various magnifications (4 μm and 2 μm). As shown in Figure 4 a, b, it is observed to be aggregated in clusters and porous structures, which indicates a greater surface area, which may increase its potential impact.

Energy dispersive X-ray spectroscopy

As shown in Figure 5, the elements present in the ZnONP sample release distinct X-ray energy, as reflected by the peaks in the energy dispersive X-ray Spectroscopy (EDXS) spectrum. The observed primary elements are Oxygen (O), Carbon (C) and Zinc (Zn). At approximately 0.3 keV, the peak represents the presence of carbon (the carbon coating commonly used in SEM/EDXS could be the cause). At approximately 0.5 keV, the peak represents the presence of oxygen (it shows the existence of oxides in the material ZnO). The two conspicuously falling within the energy range of 1.0 keV to 9.0 keV represent the presence of zinc. The higher intensity of the zinc peaks compared with those of the

Table 1: FTIR spectral peaks of the ZnONPs.

Sl. No.	Absorption peak cm–1 in znonps	Bond/ functional groups
1	3194.739	O-H stretching vibrations
2	1628.567	H-O-H bending vibrations
3	1425.88	C-H bending or symmetric COO- stretch
4	1058.589	C-O stretching vibrations
5	525.646	Zn- O stretching vibrations
6	421.489	Zn- O stretching vibrations
7	406.482	Zn- O stretching vibrations

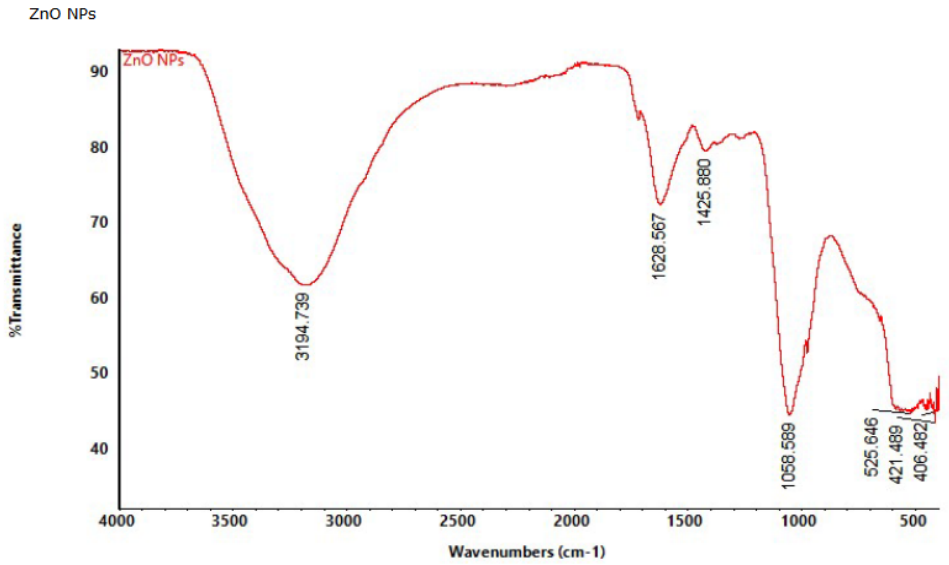

Figure 2: FTIR spectrum of the ZnONPs.

other samples indicates that zinc is the dominant component of the sample.

Antioxidant activity

DPPH Assay

Figure 6 and Table 2 present the DPPH free radical scavenging activity across concentrations ranging from 10 µg to 50 µg. The inhibition rate of the standard at a concentration of 50 µL was 95.18%, whereas that of the ZnONP was 89.47%. Moreover, at a lower concentration of 10 µL, it was 69.24%, whereas the percentage of ZnONP was 65.92%. Therefore, at both high and slow concentrations, ZnONP are slightly less potent than the standard. The IC_{50} values of the standard and ZnONP were 21.71 µg/mL and 19.01 µg/mL, respectively.

H_2O_2 Assay

The scavenging activity of H_2O_2 free radicals at different concentrations from 10 µg to 50 µg is shown in Figure 7 and Table 3. At 50 µL of standard, the inhibition rate was 87.3%, whereas it was 85.6% for the ZnONP. At 10 µg, the inhibition rate of the standard was 58.4%, and that of the ZnONP was 49.6%. This means that ZnONP is marginally less potent than the standard. The IC_{50} of the standard was 12.41 µg/mL, and that of *K. africana* was 1.70.

ABTS Assay

Table 4 and Figure 8 show the scavenging activity of the ABTS free radical at several concentrations, ranging from 10 µg to 50 µg. The inhibition rate for the ZnONP was 91.23%, whereas that for the standard was 94.53% at 50 µg. However, at 10 µg, it was 62.54% and 67.91% for standard and ZnONP, respectively. The IC_{50} value was 8.85 for the ZnONP and 17.41 for the standard.

NO_2 Assay

The NO_2 free radical scavenging activity at various concentrations (10 µg - 50 µg) is presented in Table 5 and Figure 9. At 10 µg, the rate of inhibition was 70.65% for the standard and 68.79% for the ZnONPs. At 50 µg, the rate of inhibition was 93.67% for the standard and 87.21% for the ZnONPs. The IC_{50} values for standard and ZnONPs are 32.71 and 28.06, respectively.

FRAP Assay

As shown in Figure 10 and Table 6, the FRAP free radical scavenging activity at different concentrations ranged from 10 µg - 50 µg. The inhibition rates of the standard and ZnONPs were 74.56% and 68.45%, respectively, at 10 µg and 93.64% and 89.54%, respectively, at 50 µg. These findings indicate that K. africana is slightly less potent than the standard. The IC_{50} values of both standard and ZnONPs were 43.07 and 26.54, respectively.

Antibacterial Activity

The results of this research show that synthesized ZnO nanoparticles have antibacterial activity against various pathogenic bacteria, with measurements of the zone of inhibition in millimeters (mm), which are shown in Table 7 and Figure 11. All bacteria have the same zone of inhibition of 9 mm at all concentrations tested: 25, 50, 100 µg/mL, and the standard. While *Klebsiella sp*. had the same zone of inhibition of 9 mm at all

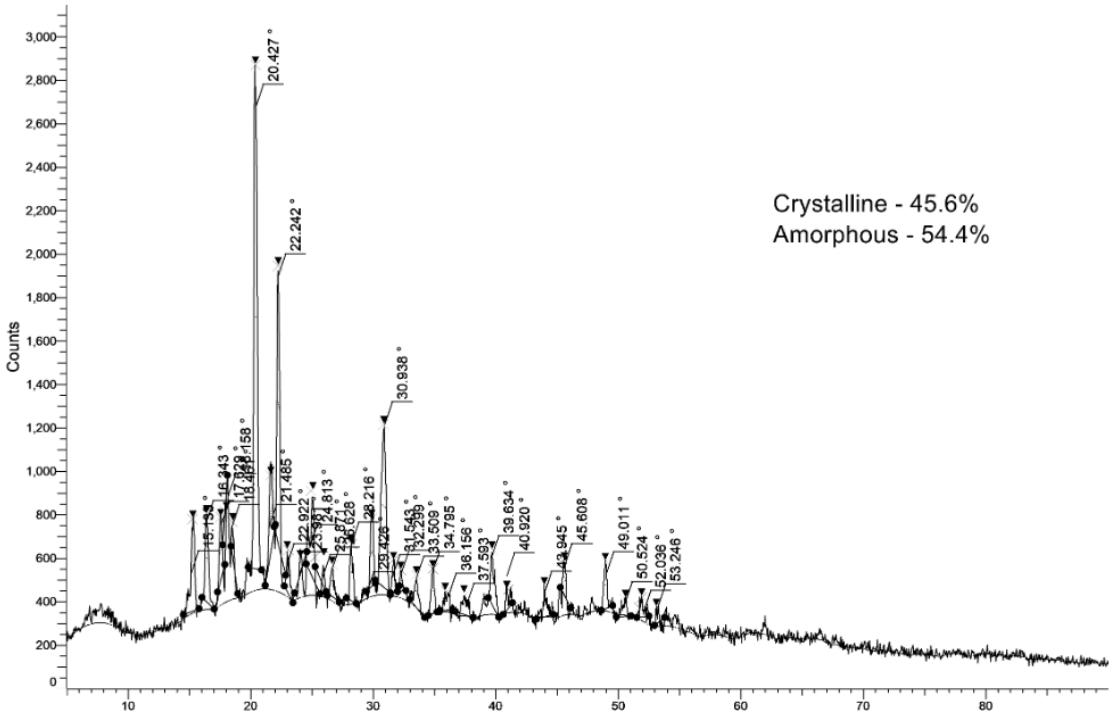

Figure 3: XRD patterns of ZnONPs.

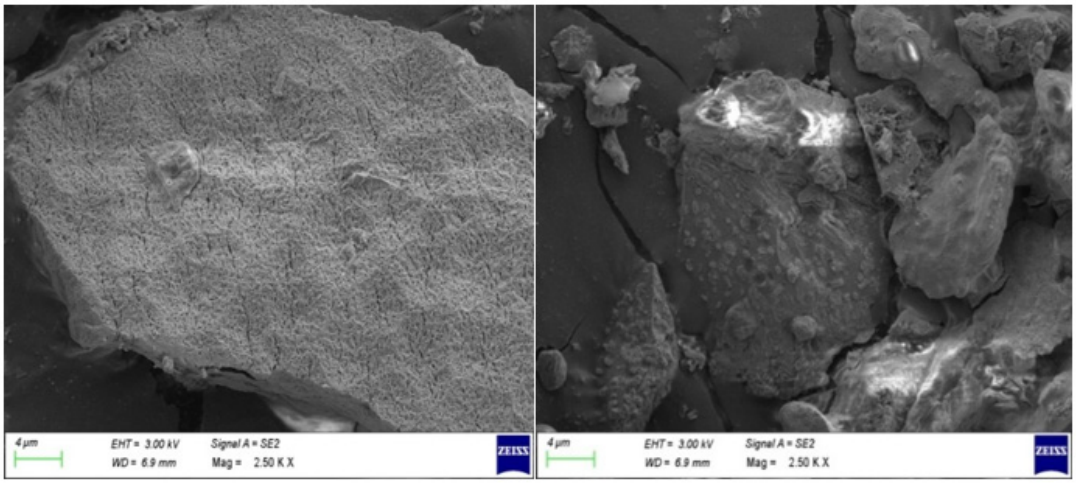

a) at 4 µm magnification

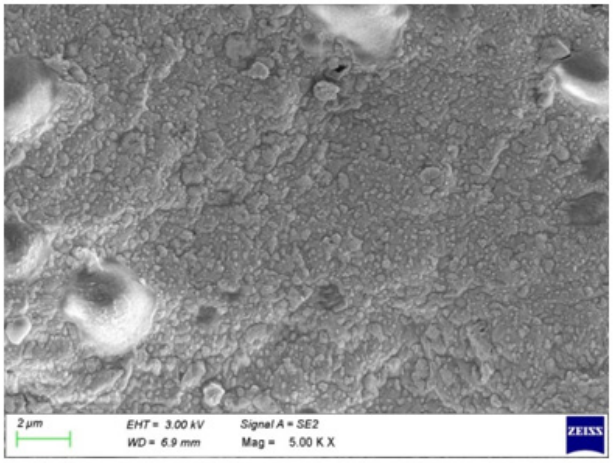

b) at 2 µm maginification

Figure 4: SEM images of ZnONPs at different magnifications.

concentrations of ZnONP tested, the standard had a greater zone of inhibition at 32 mm.

The ZnO nanoparticles seem to have a moderate but consistent antibacterial effect across all the tested bacteria at the 9 mm zone of inhibition. The inhibition zone of *Klebsiella* sp. against the standard antibiotic was considerably greater, as shown in Figure 12, indicating that, compared with the ZnO nanoparticles, the conventional treatment was significantly more efficient at inhibiting the growth of this bacterium.

DISCUSSION

Nanoparticles are ultrafine particles of plant extracts. Recently, NP have attracted increasing interest from researchers because of their various uses in various fields, such as drug delivery, electronic, magnetic, etc. Metal, metal oxide, ceramic, polymeric, lipophilic, etc., are some types of NP that are synthesized via chemical, physical and biological methods. However, owing to the high cost and toxicity of the chemicals employed in physical and chemical synthesis, various biological methods have been used. Hence, the majority of these studies focused on the biological synthesis of metallic nanoparticles. Among all metallic NP, zinc oxide NP are attractive because of their unique and advantageous properties (Pandit *et al*., 2022).

This work elaborates on the preparation of ZnONP from *Kigelia africana* fruit extract and observes their antibacterial and antioxidant effects. The extract consists of a wide range of bioactive substances, including tannins, flavonoids and saponins (Siva *et al*., 2020). Characterization of the NP was performed via various techniques: UV-visible spectroscopy, Fourier Transform Infrared (FTIR) spectroscopy, X-Ray Diffraction (XRD), Scanning Electron Microscopy (SEM), and Energy Dispersive X-Ray Spectroscopy (EDXS). UV-vis spectroscopy revealed characteristic absorption peaks to verify the effectiveness

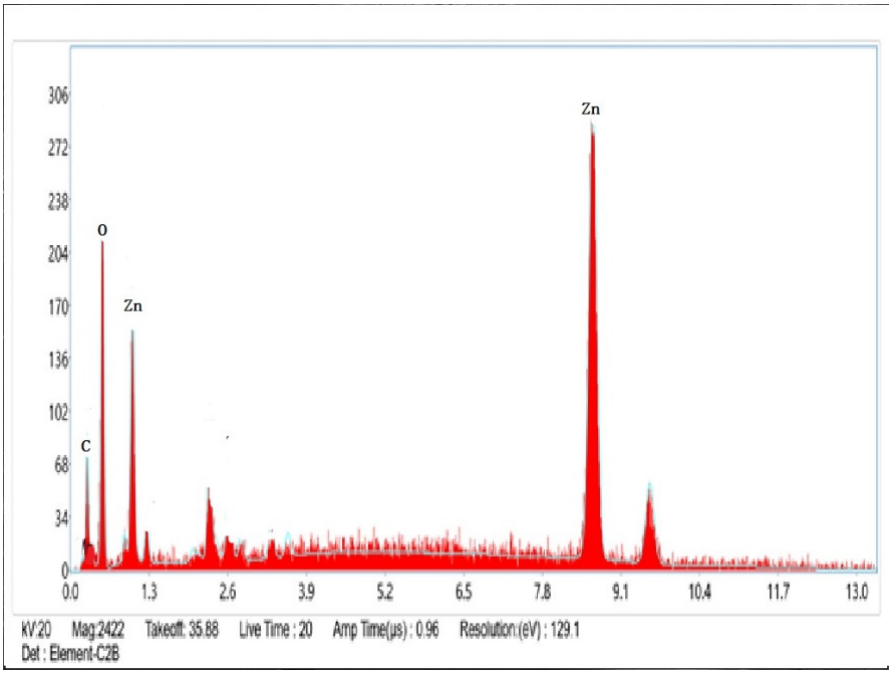

Figure 5: EDXS of ZnONPs.

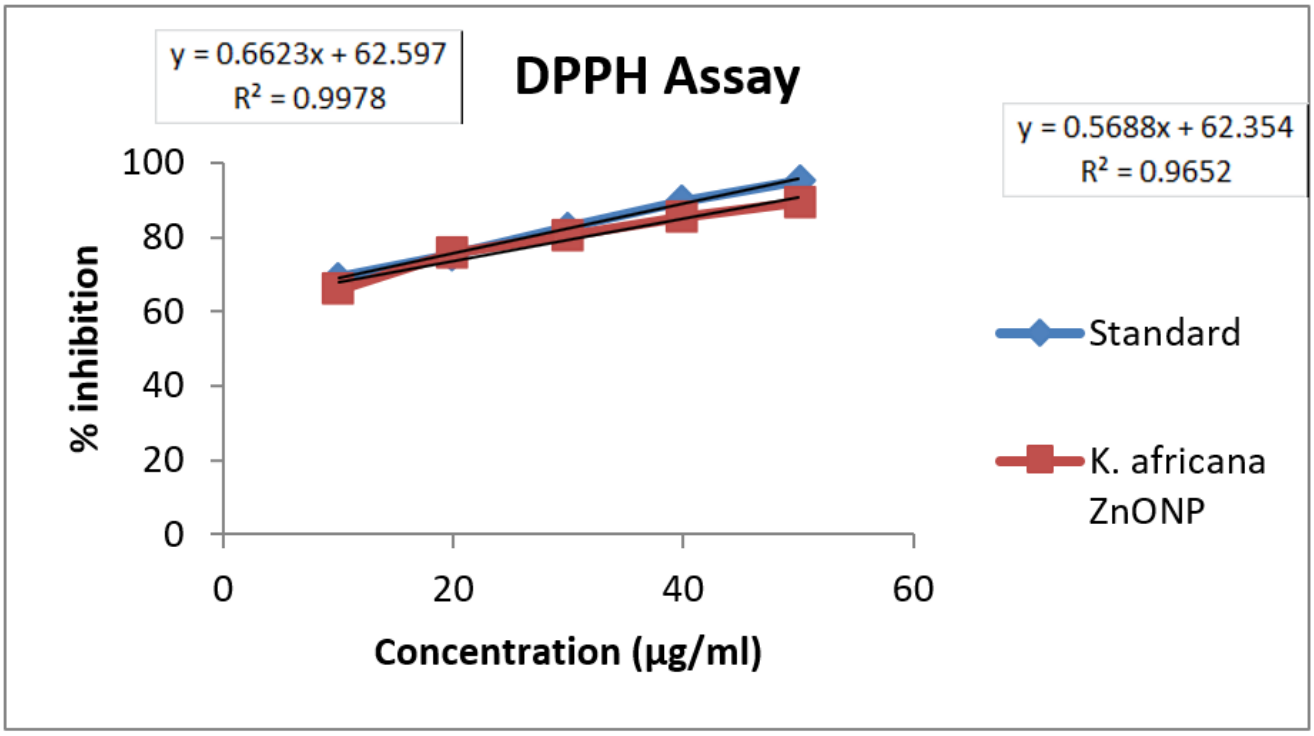

Figure 6: DPPH assay of ZnONPs.

Table 2: DPPH assay of ZnONPs.

Sl. No.	Conc.	Standard	ZnONP
1	10	69.24	65.92
2	20	75.44	75.84
3	30	82.68	80.24
4	40	89.79	85.62
5	50	95.18	89.47

of the ZnONP (Pillai *et al.*, 2020). The UV spectra revealed strong absorbance at 340 nm, where the UV-vis absorbance measurements were taken at three various time intervals (3 hr, 12 hr, and 24 hr). FTIR analysis revealed functional groups associated with NPs through the detection of features at peaks such as 3194.739 cm^{-1}, 1632.567 cm^{-1}, 1425.680 cm^{-1}, 1066.590 cm^{-1}, 525.646 cm^{-1}, 421.489 cm^{-1}, and 400.482 cm^{-1}, corresponding to O-H, H-O-H, C-H, C-O and Zn-O stretching, confirming the presence of the ZnONP. The XRD analysis of ZnONP revealed distinct diffraction peaks at 2θ values ranging from 15.13° to 53.24°, with the strongest peak at approximately 20.42° and the other prominent peaks at 22.24°and 30.93°. The Bragg reflections for prominent peaks correspond to known ZnONP crystalline planes, confirming the presence of ZnONP according to standard JCPDS 36- 1451. Using Scherrer's equation, the average size is estimated to range between 113 nm and 884 nm. SEM images used to examine the surface morphology and structure of the NP at distinct magnifications of approximately 2 µm and 4 µm revealed that the nanoparticles had aggregated and clustered surfaces, which may have enhanced their antibacterial and antioxidant effects. EDXS was used to determine the elemental composition of the sample by measuring the characteristic X-rays emitted from the elements, and for the ZnONP, at approximately 0.3 eV and 0.5 eV, the peaks represented the presence of C and O, whereas Zn presented strong peaks between 1.0 eV and 9.0 eV.

Antioxidants are substances that inhibit or reduce cell destruction caused by free radicals, which are unbalanced molecules formed by the body due to the environment or other stressors. By donating electrons to free radicals, antioxidants prevent cellular damage that leads to aging and diseases such as cancer, cardiovascular issues, and neurological diseases. The antioxidant properties were assessed through several FRAP, DPPH, H_2O_2, ABTS, and NO_2 assays (Nagajyothi *et al.*, 2015). The results of the DPPH assay revealed that the percentages of ZnONP and standard were 89.47% and 95.18%, respectively, at a concentration of 50 µL but 65.92% and 69.24%, respectively, at a concentration of 10 µL. The IC_{50} values of ZnONPs and the standard were 19.01 µg/mL and 21.71 µg/mL, respectively. In the H_2O_2 scavenging activity test, standard and ZnONPs reached 87.3% and 85.6%, respectively,

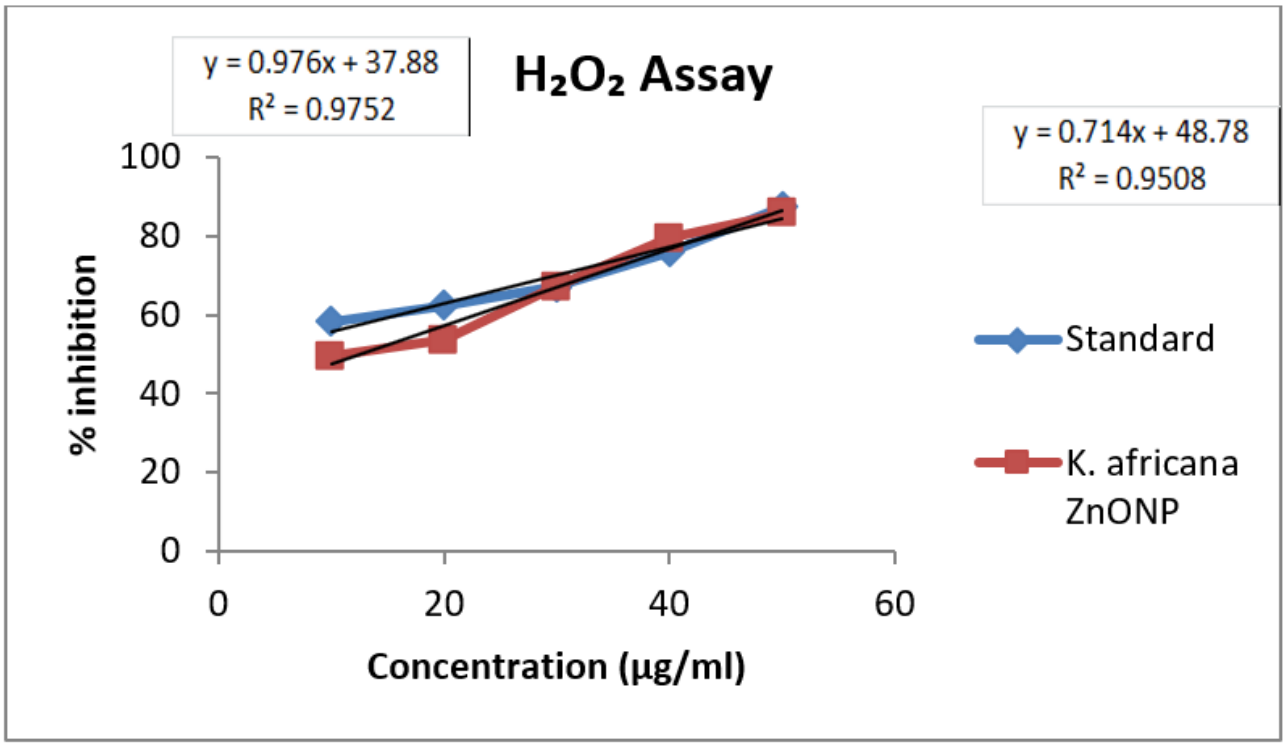

Figure 7: H_2O_2 assay of ZnONPs.

Table 3: H_2O_2 assay of ZnONPs.

Sl. No.	Conc.	Standard	ZnONP
1	10	58.4	49.6
2	20	62.3	53.8
3	30	67.1	67.4
4	40	75.9	79.4
5	50	87.3	85.6

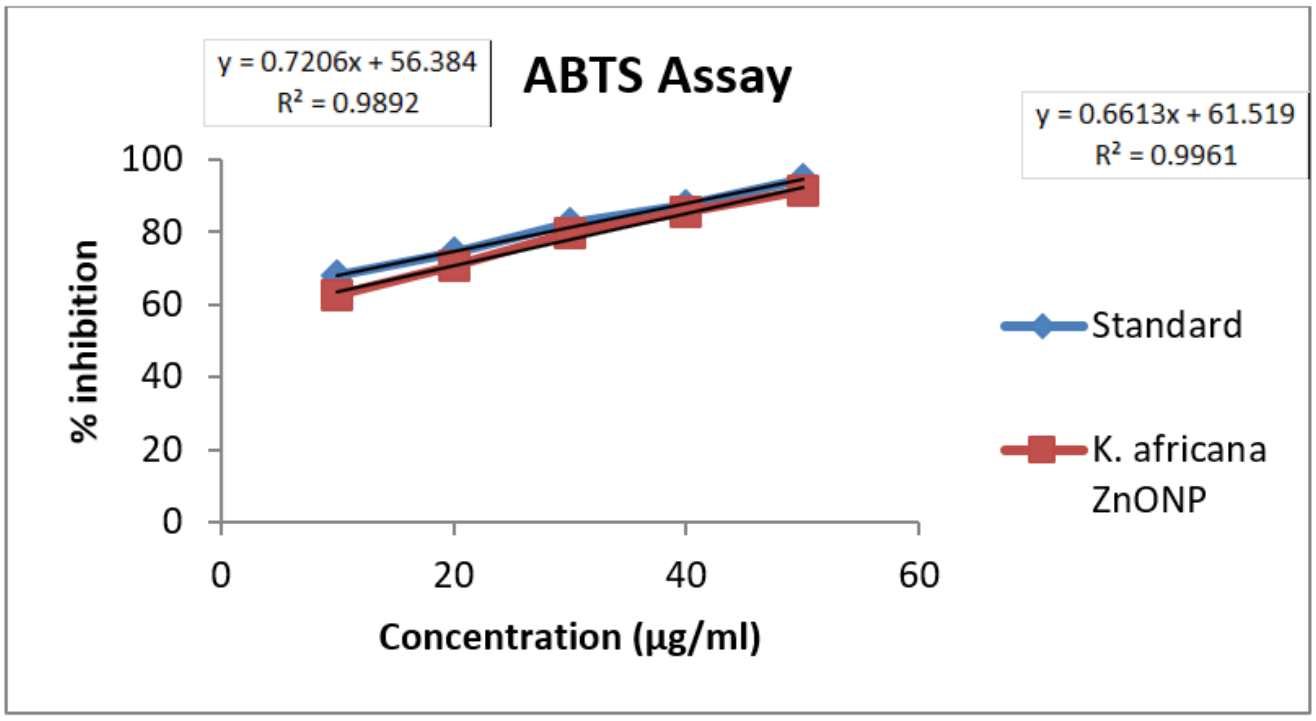

Figure 8: ABTS assay of ZnONPs.

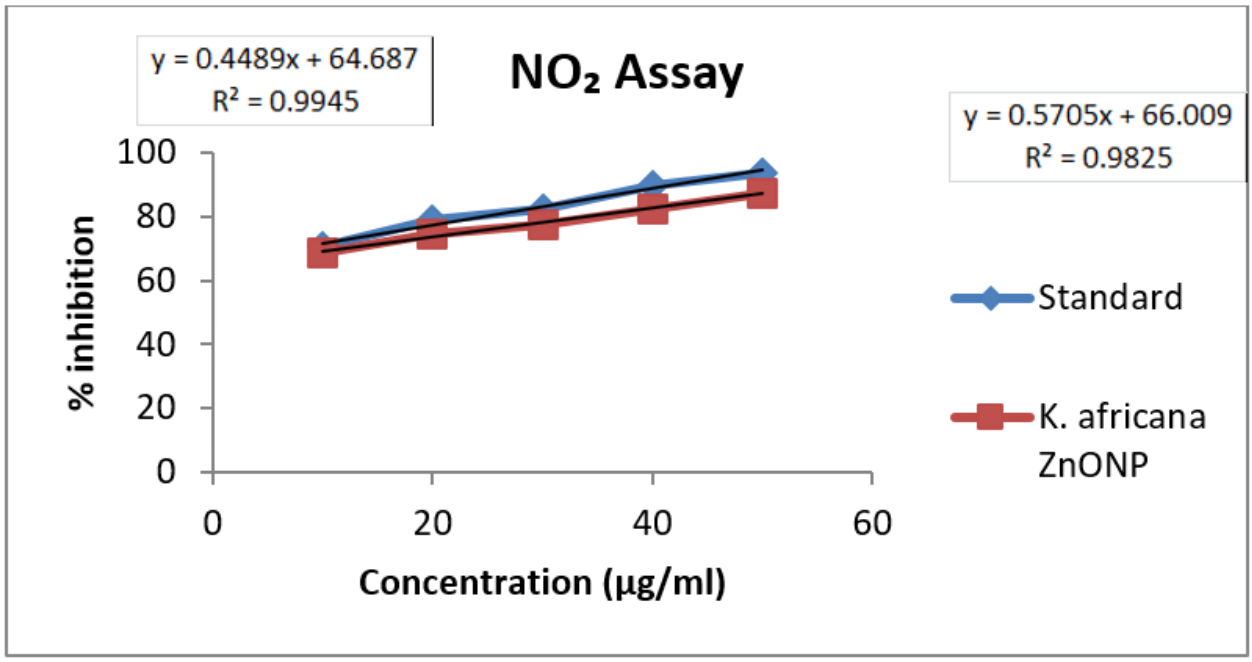

Figure 9: NO_2 assay of ZnONPs.

Table 4: ABTS assay of ZnONPs.

Sl. No.	Conc.	Standard	ZnONP
1	10	67.92	62.54
2	20	74.48	70.91
3	30	82.47	79.74
4	40	87.39	85.59
5	50	94.53	91.23

Table 5: NO_2 assay of ZnONPs.

SL. No.	Conc.	Standard	ZnONP
1	10	70.65	68.79
2	20	78.92	74.52
3	30	82.45	77.68
4	40	89.93	82.57
5	50	93.67	87.21

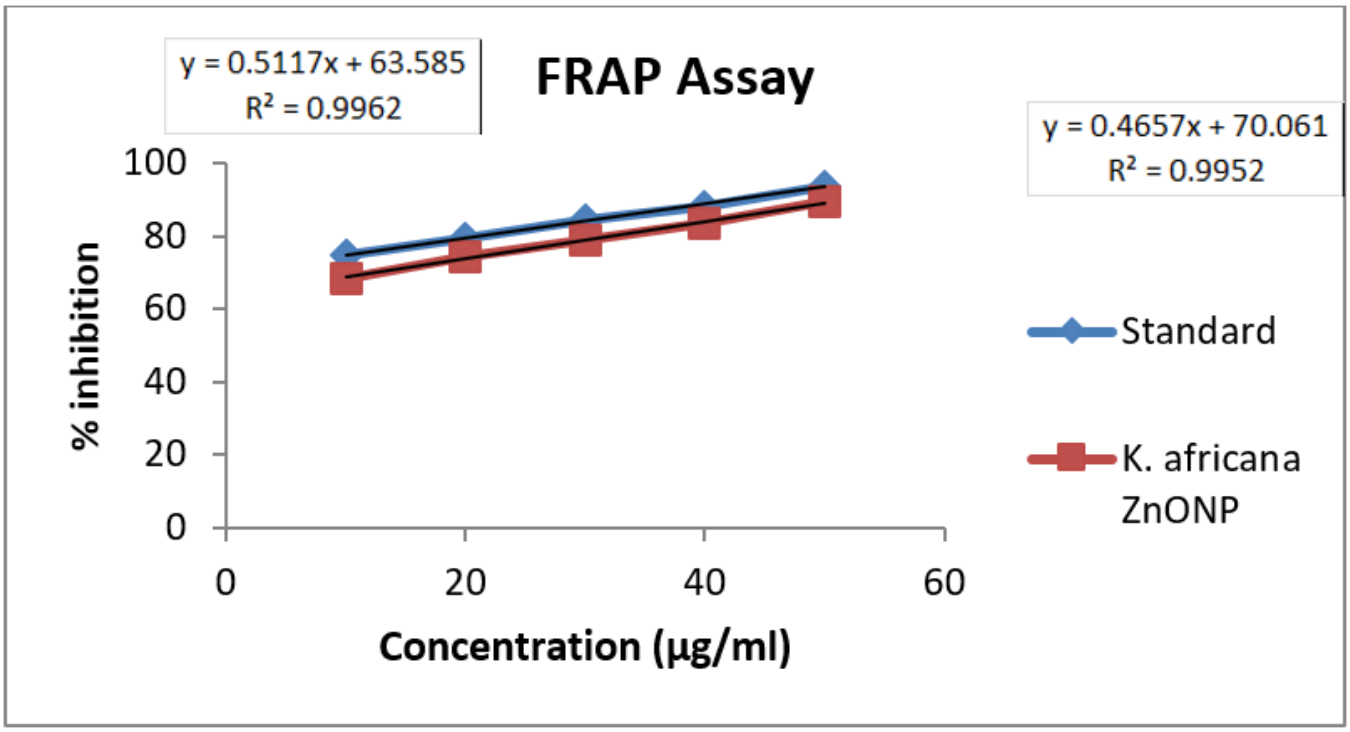

Figure 10: FRAP assay of ZnONPs.

at a concentration of 50 µL and 58.4% and 49.6%, respectively, at a concentration of 10 µL. The IC_{50} values were 12.41 µg/mL and 1.70 µg/mL for the standard and ZnONPs, respectively. The results of the ABTS free radical scavenging test revealed that, at a lower concentration of 10 µL, 67.91% and 62.54% were achieved by standard and ZnONP, respectively, and at a higher concentration of 50 µL, 94.53% and 91.23% were achieved by standard and ZnONP, respectively. Additionally, the IC_{50} values for standard and ZnONP were determined to be 17.41 µg/mL and 8.85 µg/mL, respectively. According to the NO_2 assay, the standard and ZnONP reached 93.67% and 87.21%, respectively, at high concentrations of 50 µL and 70.65% and 68.79%, respectively, at lower concentrations of 10 µL. Furthermore, the IC_{50} values for standard and ZnONP were 32.71 and 28.06, respectively. The FRAP test revealed that at 10 µL and 50 µL, the standard and ZnONP mixtures achieved 74.56% and 93.64% and 68.45% and 89.54%, respectively. Additionally, the IC_{50} values were 43.07 µg/mL and 26.54 µg/mL for the standard and ZnONP, respectively.

The antibacterial activity of ZnONP was tested by using four bacterial strains *Enterococcus faecalis, Escherichia coli, Staphylococcus aureus*, and *Klebsiella sp*. The efficiency of various concentrations of ZnONP, such as 25, 50, and 100 µg/mL, was evaluated via the agar well diffusion technique in comparison with that of a common antibiotic control (chloramphenicol) (Liu *et al.*, 2009). The ZnONP had a consistent zone of inhibition of approximately 9 mm for all the studied bacteria (excluding *Klebsiella* sp.) at all concentrations. This consistency points to the mild but consistent antibacterial impact of the ZnONP. At all the tested concentrations, *Klebsiella* sp. displayed a similar 9 mm inhibition zone; however, in comparison with the standard antibiotic (chloramphenicol), it demonstrated a superior inhibition effect, especially for *Klebsiella* sp., with a zone of inhibition significantly greater than that observed for the ZnONP.

Table 6: FRAP assay of ZnONPs.

SL. No.	Conc.	Standard	ZnONP
1	10	74.56	68.45
2	20	79.49	74.47
3	30	84.57	78.76
4	40	87.9	83.46
5	50	93.64	89.54

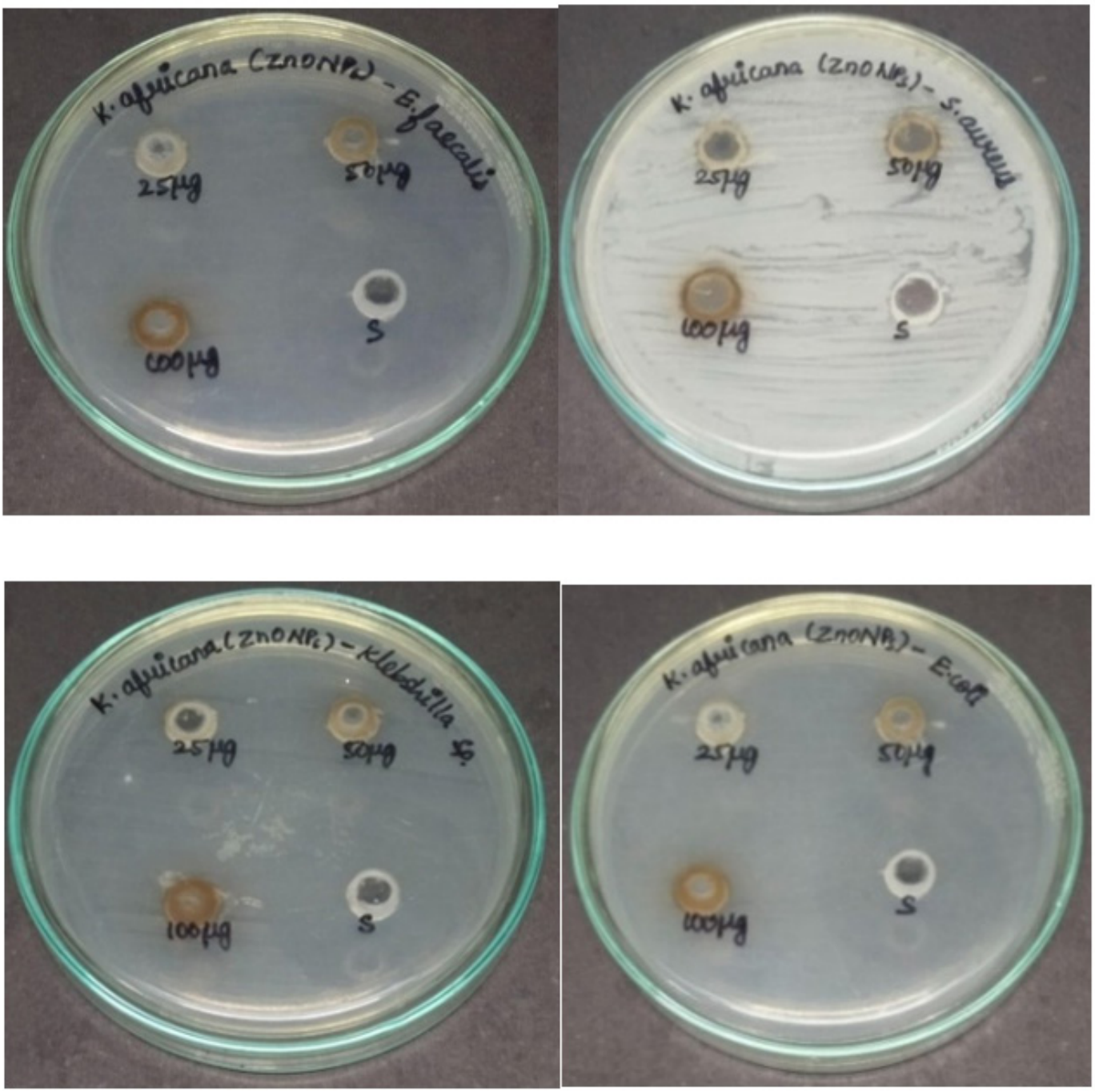

Figure 11: Antibacterial activity of ZnONPs of *Kigelia africana* against *E. faecalis, E. coli*, S. *aureus* and *Klebsiella sp.*

Table 7: Antibacterial activity of ZnONPs against pathogenic bacteria and their zones of inhibition.

Sl. No.	Organism	Concentration	Zone of inhibition
1	*E. faecalis*	25	9
		50	9
		100	9
		Standard	9
2	*E. coli*	25	9
		50	9
		100	9
		Standard	9
3	*S. aureus*	25	9
		50	9
		100	9
		Standard	9
4	*Klebsiella* sp.	25	9
		50	9
		100	9
		Standard	32

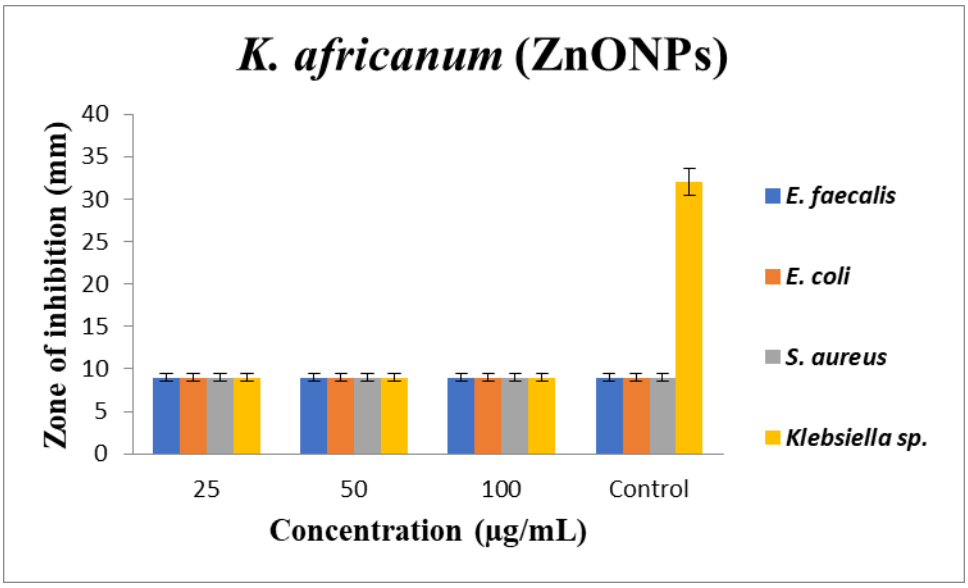

Figure 12: Zone of inhibition of ZnONPs.

CONCLUSION

This study describes the synthesis of zonc oxide nanoparticles from *Kigelia africana* fruit extract. Bioactive components such as iridoids, alkaloids, quinones, and steroids are found in the fruits of *Kigelia africana*. ZnONP have antioxidant, hydroxyl radical, hydrogen peroxide, and superoxide scavenging activities. This activity is due to the functional groups present in the ZnONP. Moreover, because of their small size and ability to act as capping agents, ZnONP exhibit potent antibacterial action against selected bacteria. Since these zinc oxide nanoparticles are nontoxic, inexpensive, environmentally friendly, and highly effective against bacteria, they might be employed as antibiotics in the future.

FUTURE PERSPECTIVE

Incorporating ZnONPs into nanocarriers for targeted drug delivery in cancer and other diseases. Integration into biosensors for real-time detection of pathogens or biomarkers. Exploration of their role in tissue engineering, such as creating scaffolds with enhanced antibacterial and antioxidant activity testing

biocompatibility and efficacy through *in vivo* studies for safety in human applications. Evaluating long-term effects and stability in therapeutic and cosmetic formulations

ACKNOWLEDGEMENT

The authors express their thanks and gratitude to Saveetha Institute Medical and Technical Science, Thandalam, for providing support for publishing this research article. The graphical abstract was created by using BioRender.com (https://biorender.com/).

CONFLICT OF INTEREST

The authors declare that there is no conflict of interest.

ABBREVIATIONS

FTIR: Fourier transform infrared spectroscopy; **XRD:** X-ray diffraction; **SEM:** Scanning electron microscopy; **EDXS:** Energy dispersive X-ray spectroscopy; **DPPH:** 2,2-diphenyl-1-picrylhydrazyl; **H_2O_2:** Hydrogen peroxide; **ABTS:** Azinobis-3-ethylbenzothiazoline-6-sulfonic acid; **FRAP:** Ferric reducing antioxidant power; **NO_2:** Nitric oxide.

REFERENCES

Abbasi, B. A., Iqbal, J., Ahmad, R., Zia, L., Kanwal, S., Mahmood, T., Wang, C., & Chen, J.-T. (2019). Bioactivities of *geranium wallichianum* leaf extracts conjugated with zinc oxide nanoparticles. Biomolecules, 10(1), Article 38. https://doi.org/10.3390/biom10010038

Al Awadh, A. A., Shet, A. R., Patil, L. R., Shaikh, I. A., Alshahrani, M. M., Nadaf, R., Mahnashi, M. H., Desai, S. V., Muddapur, U. M., Achappa, S., Hombalimath, V. S., Khan, A. A., Gouse, H. S. M., Iqubal, S. M. S., & Kumbar, V. (2022). Sustainable synthesis and characterization of zinc oxide nanoparticles using *Raphanus sativus* extract and its biomedical applications. Crystals, 12(8). https://doi.org/10.3390/cryst12081142

Anandhi, P., Tharani, M., Rajeshkumar, S., & Lakshmi, T. (2022). Antibacterial activity of cinnamon and clove oil against wound pathogens. Journal of Population Therapeutics and Clinical Pharmacology [Journal de la Thérapeutique des Populations et de la Pharmacologie Clinique], 28(2), e41–e46. https://doi.org/10.47750/jptcp.2022.871

Arena, K., Rigano, F., Mangraviti, D., Cacciola, F., Occhiuto, F., Dugo, L., Dugo, P., & Mondello, L. (2020). Exploration of rapid evaporative-ionization mass spectrometry as a shotgun approach for the comprehensive characterization of *Kigelia africana* (Lam.) Benth. fruit. Molecules, 25(4), Article 962. https://doi.org/10.3390/molecules25040962

Ashwini, J., Aswathy, T. R., Rahul, A. B., Thara, G. M., & Nair, A. S. (2021). Synthesis and characterization of zinc oxide nanoparticles using *acacia caesia* bark extract and its photocatalytic and antimicrobial activities. Catalysts, 11(12). https://doi.org/10.3390/catal11121507

Chukwudozie, I. K., & Ezeonu, I. M. (2022). Antimicrobial properties and acute toxicity evaluation of *Pycnanthus angolensis* stem bark. Scientific African, 16. https://doi.org/10.1016/j.sciaf.2022.e01185

Demissie, M. G., Sabir, F. K., Edossa, G. D., & Gonfa, B. A. (2020). Synthesis of zinc oxide Nanoparticles Using Leaf Extract of *Lippia adoensis* (Koseret) and Evaluation of Its antibacterial activity. Journal of Chemistry, 2020, 1–9. https://doi.org/10.1155/2020/7459042

Deng, J., Cheng, W., & Yang, G. (2011). A novel antioxidant activity index (AAU) for natural products using the DPPH assay. Food Chemistry, 125(4), 1430–1435. https://doi.org/10.1016/j.foodchem.2010.10.031

Dhandapani, K. V., Anbumani, D., Gandhi, A. D., Annamalai, P., Muthuvenkatachalam, B. S., Kavitha, P., & Ranganathan, B. (2020). Green route for the synthesis of zinc oxide nanoparticles from *Melia azedarach* leaf extract and evaluation of their antioxidant and antibacterial activities. Biocatalysis and Agricultural Biotechnology, 24. https://doi.org/10.1016/j.bcab.2020.101517

Dlamini, N. G., Basson, A. K., & Pullabhotla, V. S. R. (2023). Synthesis and characterization of various bimetallic nanoparticles and their application. Applied Nano, 4(1), 1–24. https://doi.org/10.3390/applnano4010001

Dua, T. K., Giri, S., Nandi, G., Sahu, R., Shaw, T. K., & Paul, P. (2023). Green synthesis of silver nanoparticles using *Eupatorium adenophorum* leaf extract: Characterizations, antioxidant, antibacterial and photocatalytic activities. Chemicke Zvesti, 77(6), 2947–2956. https://doi.org/10.1007/s11696-023-02676-9

Happy, A., Soumya, M., Venkat Kumar, S., Rajeshkumar, S., Sheba, R. D., Lakshmi, T., & Deepak Nallaswamy, V. (2019). Phyto-assisted synthesis of zinc oxide nanoparticles using *Cassia alata* and its antibacterial activity against *Escherichia coli*. Biochemistry and Biophysics Reports, 17, 208–211. https://doi.org/10.1016/j.bbrep.2019.01.002

Houghton, P. J., & Jâger, A. K. (2002). The sausage tree (*Kigelia pinnata*): Ethnobotany and recent scientific work. South African Journal of Botany, 68(1), 14–20. https://doi.org/10.1016/S0254-6299(15)30434-8

I, S. T., Pitchiah, S., Suresh, V., & Ramasamy, P. (2023). Synthesis of zinc oxide nanoparticles from aqueous extract of *Avicennia marina* mangrove leaves and their antibacterial activities against oral pathogens. Cureus, 15(10), Article e47627. https://doi.org/10.7759/cureus.47627

Jayachandran, A., T R, A., & Nair, A. S. (2021). Green synthesis and characterization of zinc oxide nanoparticles using *Cayratia pedata* leaf extract. Biochemistry and Biophysics Reports, 26, Article 100995. https://doi.org/10.1016/j.bbrep.2021.100995

Jency Evanjelin, P., Uma Maheswari, T. N., Pillai, D. S., & Rajeshkumar, S. (2023). Green synthesis of zinc oxide nanoparticles from *Phoenix dactylifera* and their anti-microbial potentiality-An *in vitro* study. Biomedicine, 43(4), 1226–1230. https://doi.org/10.51248/.v43i4.2230

Jeyabharathi, S., Naveenkumar, S., Chandramohan, S., Venkateshan, N., Gawwad, M. R. A., Elshikh, M. S., Rasheed, R. A., Al Farraj, D. A., & Muthukumaran, A. (2022). Biological synthesis of zinc oxide nanoparticles from the plant extract, *Wattakaka volubilis* showed anti-microbial and anti-hyperglycemic effects. Journal of King Saud University – Science, 34(3). https://doi.org/10.1016/j.jksus.2022.101881

Kayani, W. K., Dilshad, E., Ahmed, T., Ismail, H., & Mirza, B. (2016). Evaluation of *Ajuga bracteosa* for antioxidant, anti-inflammatory, analgesic, antidepressant and anticoagulant activities. BMC Complementary and Alternative Medicine, 16(1), 375. https://doi.org/10.1186/s12906-016-1363-y

Kokate, M., Garadkar, K., & Gole, A. (2016). Zinc-oxide-silica–silver nanocomposite: Unique one-pot synthesis and enhanced catalytic and anti-bacterial performance. Journal of Colloid and Interface Science, 483, 249–260. https://doi.org/10.1016/j.jcis.2016.08.039

Liu, Y., He, L., Mustapha, A., Li, H., Hu, Z. Q., & Lin, M. (2009). Antibacterial activities of zinc oxide nanoparticles against *Escherichia coli* O157:H7. Journal of Applied Microbiology, 107(4), 1193–1201. https://doi.org/10.1111/j.1365-2672.2009.04303.x

Manikanika, & Chopra, L. (2023). Photo-degradation of dyes and drugs using Aloe vera synthesized zinc oxide nanoparticles-A review. Materials Today: Proceedings, 72, 1613–1617. https://doi.org/10.1016/j.matpr.2022.09.413

Nagajyothi, P. C., Cha, S. J., Yang, I. J., Sreekanth, T. V. M., Kim, K. J., & Shin, H. M. (2015). Antioxidant and anti-inflammatory activities of zinc oxide nanoparticles synthesized using *Polygala tenuifolia* root extract. Journal of Photochemistry and Photobiology. B, Biology, 146, 10–17. https://doi.org/10.1016/j.jphotobiol.2015.02.008

Narath, S., Koroth, S. K., Shankar, S. S., George, B., Mutta, V., Wacławek, S., Černík, M., Padil, V. V. T., & Varma, R. S. (2021). *Cinnamomum tamala* Leaf Extract Stabilized Zinc Oxide Nanoparticles: A Promising Photocatalyst for Methylene Blue Degradation. Nanomaterials, 11(6), Article 1558. https://doi.org/10.3390/nano11061558

Nouren, S., Bibi, I., Kausar, A., Sultan, M., Nawaz Bhatti, H., Safa, Y., Sadaf, S., Alwadai, N., & Iqbal, M. (2024). Green synthesis of CuO nanoparticles using Jasmin sambac extract: Conditions optimization and photocatalytic degradation of methylene blue dye. Journal of King Saud University – Science, 36(3). https://doi.org/10.1016/j.jksus.2024.103089

Osman, A., Ali, Z., Chittiboyina, A., & Khan, I. (2017). *Kigelia africana* fruit: Constituents, bioactivity, and reflection on composition disparities. World Journal of Traditional Chinese Medicine, 3(4). https://doi.org/10.4103/wjtcm.wjtcm_15_17

Pachaiappan, R., Rajendran, S., Ramalingam, G., Vo, D.-V. N., Priya, P. M., & Soto-Moscoso, M. (2021). Green synthesis of zinc oxide nanoparticles by *Justicia adhatoda* Leaves and Their antimicrobial activity. Chemical Engineering and Technology, 44(3), 551–558. https://doi.org/10.1002/ceat.202000470

Pandit, C., Roy, A., Ghotekar, S., Khusro, A., Islam, M. N., Emran, T. B., Lam, S. E., Khandaker, M. U., & Bradley, D. A. (2022). Biological agents for synthesis of nanoparticles and their applications. Journal of King Saud University – Science, 34(3). https://doi.org/10.1016/j.jksus.2022.101869

Perera, W. P. T. D., Dissanayake, R. K., Ranatunga, U. I., Hettiarachchi, N. M., Perera, K. D. C., Unagolla, J. M., De Silva, R. T., & Pahalagedara, L. R. (2020). Curcumin loaded zinc oxide nanoparticles for activity-enhanced antibacterial and anticancer applications. RSC Advances, 10(51), 30785–30795. https://doi.org/10.1039/d0ra05755j

Pillai, A. M., Sivasankarapillai, V. S., Rahdar, A., Joseph, J., Sadeghfar, F., Anuf A, R., Rajesh, K., & Kyzas, G. Z. (2020). Green synthesis and characterization of zinc oxide nanoparticles with antibacterial and antifungal activity. Journal of Molecular Structure, 1211. https://doi.org/10.1016/j.molstruc.2020.128107

Purbowati, R., Pratiwi, V. M., Masfufatun, M., Tania, P. O. A., & Khumaeni, A. (2023). Antibacterial and antibiofilm effects of gold and silver nanoparticles against the uropathogenic *Escherichia coli* by scanning electron microscopy (SEM) analysis. Healthcare in Low-Resource Settings, 11(2). https://doi.org/10.4081/hls.2023.11748

Re, R., Pellegrini, N., Proteggente, A., Pannala, A., Yang, M., & Rice-Evans, C. (1999). Antioxidant activity applying an improved ABTS radical cation decolorization assay. Free Radical Biology and Medicine, 26 (9–10), 1231–1237. https://doi.org/10.1016/S0891-5849(98)00315-3

Singh, S., & Tripathi, A. (2018). Collection, identification, molecular characterization, and antioxidant activity of non-gilled mushrooms collected from north western Himalayas. Asian Journal of Pharmaceutical and Clinical Research, 11(10). https://doi.org/10.22159/ajpcr.2018.v11i10.27423

Siva, R., Valarmathi, T. N., Palanikumar, K., & Samrot, A. V. (2020). Study on a Novel natural cellulosic fiber from *Kigelia africana* fruit: Characterization and analysis. Carbohydrate Polymers, 244, Article 116494. https://doi.org/10.1016/j.carbpol.2020.116494

Sorbiun, M., Shayegan Mehr, E., Ramazani, A., & Mashhadi Malekzadeh, A. (2018). Biosynthesis of metallic nanoparticles using plant extracts and evaluation of their antibacterial properties. Nanochemistry Research, 3(1), 1–16. https://doi.org/10.22036/ncr.2018.01.001

Taranath, T. C., & Patil, B. N. (2016). *Limonia acidissima* L. leaf mediated synthesis of zinc oxide nanoparticles: A potent tool against *Mycobacterium tuberculosis*. International Journal of Mycobacteriology, 5(2), 197–204. https://doi.org/10.1016/j.ijmyco.2016.03.004

Thaipong, K., Boonprakob, U., Crosby, K., Cisneros-Zevallos, L., & Hawkins Byrne, D. (2006). Comparison of ABTS, DPPH, FRAP, and ORAC assays for estimating antioxidant activity from guava fruit extracts. Journal of Food Composition and Analysis, 19 (6–7), 669–675. https://doi.org/10.1016/j.jfca.2006.01.003

Urnukhsaikhan, E., Bold, B.-E., Gunbileg, A., Sukhbaatar, N., & Mishig-Ochir, T. (2021). Antibacterial activity and characteristics of silver nanoparticles biosynthesized from *Carduus crispus*. Scientific Reports, 11(1), Article 21047. https://doi.org/10.1038/s41598-021-00520-2

Vijayakumar, N., Bhuvaneshwari, V. K., Ayyadurai, G. K., Jayaprakash, R., Gopinath, K., Nicoletti, M., Alarifi, S., & Govindarajan, M. (2022). Green synthesis of zinc oxide nanoparticles using *Anoectochilus elatus*, and their biomedical applications. Saudi Journal of Biological Sciences, 29(4), 2270–2279. https://doi.org/10.1016/j.sjbs.2021.11.065

Wali, S., Zahra, M., Okla, M. K., Wahidah, H. A., Tauseef, I., Haleem, K. S., Farid, A., Maryam, A., Abdelgawad, H., Adetunji, C. O., Akhtar, N., Akbar, S., Rehman, W., Yasir, H., & Shakira, G. (2022). *Brassica oleracea* L. (Acephala Group) based zinc oxide nanoparticles and their efficacy as antibacterial agent. Brazilian Journal of Biology, 84, Article e259351. https://doi.org/10.1590/1519-6984.259351.

Cite this article: Hindumathi DJ, Ramasamy J, Jothibasu D, Ravikumar N, Cheriyar BV, Pandi K. Exploring the Bioactivity of Zinc Oxide Nanoparticles Synthesized Using *Kigelia africana* Fruit Extract. Int. J. Pharm. Investigation. 2026;16(1):210-24.